Homework 2

TRANSONIC AERODYNAMICS

MEC6602

Authors:

Latimier Corentin (2306373)
Defer Tristan (2306485)

October 28, 2024

POLYTECHNIQUE
MONTRÉAL

Contents

Introduction **2**

1 Modelisation and numerical strategy **2**

2 Shock tube **2**
2.1 Numerical setup . . . 2
2.2 Comparison of Numerical Schemes . . . 3

3 Nozzle **3**
3.1 Numerical Setup . . . 3
3.2 Results . . . 3
3.2.1 Supersonic inlet - Supersonic outlet . . . 3
3.2.2 Supersonic inlet - Subsonic outlet . . . 4

References **5**

A Numerical schemes [1] **6**

B Results for the shock tube **8**

C Results for the Nozzle : Supersonic inlet - Supersonic outlet **10**
C.1 MacCormack scheme . . . 10
C.2 Lax-Wendroff scheme . . . 13
C.3 Implicit Beam-Warming scheme . . . 15

D Results for the Nozzle : Supersonic inlet - Subsonic outlet **17**
D.1 MacCormack scheme . . . 17
D.2 Lax-Wendroff scheme . . . 19

Introduction

In this study, we solve the 1D Euler equations [1] for two classical fluid dynamics problems: the Sod shock tube and a quasi-1D nozzle. The Sod shock tube is an unsteady problem involving shock waves and expansion fans, making it a good test for evaluating numerical methods. The quasi-1D nozzle is a stationary problem that models how air flows through a nozzle, particularly useful for studying transonic flows with shock waves.

We apply three different numerical schemes to these problems and compare the results with theoretical solutions. The goal is to assess the accuracy and performance of each scheme in capturing the important flow features, especially in transonic conditions where shocks and discontinuities are common.

1 Modelisation and numerical strategy

In conservative form, the quasi 1D Euler equations are:

$$\frac{\partial \vec{Q}}{\partial t} + \frac{\partial \vec{E}}{\partial x} = \vec{S} \tag{1}$$

where $\vec{Q} = \begin{bmatrix} \rho A \\ \rho u A \\ \rho E A \end{bmatrix}$ is the vector of conserved variables, $\vec{E} = \begin{bmatrix} \rho u A \\ (\rho u^2 + p) A \\ u(\rho E + p) A \end{bmatrix}$ is the flux vector and $\vec{S} = \begin{bmatrix} 0 \\ p \frac{dA}{dx} \\ 0 \end{bmatrix}$ is the source term vector.

In these equations, ρ is the fluid density, u is the fluid velocity in the x-direction, p is the pressure, E is the total energy ($E = e + \frac{1}{2}u^2$, where e is the internal energy), p is the pressure and A is the area of the domain.

To close the system of equations, a thermodynamic relation must be added. In this work, the perfect gas law is used:

$$p = (\gamma - 1)\left[\rho E - \frac{1}{2}\rho u^2\right]$$

In this work, three numerical schemes are evaluated: the **Mac-Cormack** scheme, the **Lax-Wendroff** scheme, and the **implicit Beam-Warming** scheme wich are all detailled in appendix A.

2 Shock tube

This section focuses on analyzing the behavior of a fluid inside a shock tube with a length $L = 1000$ and a constant cross-sectional area $A = 1$. The fluid is initially at rest, with different initial conditions on either side of the midpoint $x = 500$:

- For $x < 500$, the fluid has a density $\rho = 4$ and pressure $p = 4$.
- For $x > 500$, the density is $\rho = 1$ and the pressure is $p = 1$.

Since the cross-sectional area of the shock tube remains constant throughout the domain, the source term in the governing equations is equal to zero.

2.1 Numerical setup

The computational domain is discretized into 500 uniformly spaced cells. The time step is dynamically computed based on the user's specified CFL condition, ensuring stability for the numerical schemes. The time step is given by:

$$\Delta T = \min_i \left(\frac{\text{CFL} \times \Delta x}{|u_i| + c_i} \right)$$

where Δx is the grid spacing, u_i is the fluid velocity, and c_i is the local speed of sound in cell i.

In the results, CFL number is set to 0.6.

For the Beam-Warming scheme, the explicit dissipation is set to 0.05, while the implicit dissipation is configured to be twice that value. In this section, the numerical schemes are initially compared, and the results are evaluated against the analytical solution. In the second part, the impact of the dissipation coefficients, ϵ_i and ϵ_e, on the Beam-Warming scheme is analyzed.

2.2 Comparison of Numerical Schemes

The results for each of the three numerical schemes are shown in Figures 1, 2, 3, 4, and 5 in appendix B. All schemes demonstrate strong agreement with the analytical solution. Dispersion errors are observed in both the Lax-Wendroff and MacCormack schemes, particularly near regions of high gradients, while the Beam-Warming scheme shows dissipation errors due to the inclusion of dissipation coefficients in its formulation. No notable differences are found between the MacCormack and Lax-Wendroff schemes.

3 Nozzle

This section focuses on analyzing fluid behavior within a nozzle. The problem is referred to as **Quasi 1D nozzle flow** because the variation in nozzle area is accounted for through a source term in the Euler equations.

Two cases are considered: a **supersonic inlet - supersonic outlet** case and a **supersonic inlet - subsonic outlet** case. The second case is numerically more challenging, as a shock wave is expected to form within the nozzle to accommodate the back pressure.

The area of the nozzle is defined by :

$$A(x) = 1.398 + 0.347 \tanh(0.8x - 4) \text{ with } x \in [0; 10]$$

Mach at inlet is defined as $M_\infty = 1.25$. For the subsonic case, back-pressure is defined as : $p_b = 1.9 p_\infty$

3.1 Numerical Setup

The computational domain is discretized into 200 uniformly spaced cells. Since the problem is steady, a local time step is computed for each cell based on a specified CFL number, ensuring stability for the numerical schemes. The local time step is given by:

$$\Delta T_i = \left(\frac{\text{CFL} \times \Delta x}{|u_i| + c_i} \right)$$

where: Δx is the grid spacing, u_i is the fluid velocity, and c_i is the local speed of sound in cell i.
For the following results, the CFL number is set to 0.8.

The flow inside the nozzle is initialized using the inlet conditions. A subsonic boundary condition is defined using Riemann invariants. Since the problem is steady, residuals are monitored throughout the iterations. Convergence is achieved when all residuals are below 10^{-6}. To prevent infinite computation time, a maximum iteration limit of 50,000 is also imposed.

3.2 Results

3.2.1 Supersonic inlet - Supersonic outlet

We focuses on the results in the case of a supersonic inlet and a supersonic outlet. All the results are given in appendix C. First, results obtained using the Mac-Cormack scheme are presented. The evolution of residuals over iterations is presented in 6. Approximately 1,600 iterations are required for all residuals to drop below 10^{-6}.

Figures 7 and 8 display the Mach number distribution within the nozzle. As expected, the outlet Mach number exceeds 1, indicating a supersonic flow. No shocks are observed within the nozzle. Figure 9 show the evolution of density, velocity, pressure and total energy within the nozzle.

Then, results obtained using the Lax-Wendroff scheme are presented. Evolution of residuals over iterations are presented in 10. Approximately 3,500 iterations are required for all residuals to drop below 10^{-10}.

Figures 11 and 12 present the Mach number distribution within the nozzle, showing results comparable to those obtained with the MacCormack scheme. Same observation is obtained for pressure, density, velocity and total energy distribution (Figure 13)

Finally, results obtained using the Beam-Warming scheme are presented. Evolution of residuals over iterations are presented in 14. Approximately 2,500 iterations are required for all residuals to drop below 10^{-6}.

Figures 15 and 16 present the Mach number distribution within the nozzle, showing results comparable to those obtained with the MacCormack scheme. Same observation is obtained for pressure, density, velocity and total energy distribution (Figure 17)

3.2.2 Supersonic inlet - Subsonic outlet

We now focuses on the case where the inlet of the nozzle is still supersonic, but now the outlet is subsonic, therefore we expect a shock to happen in the nozzle. First, we look at the results given by the MacCormack scheme.

The residuals evolution over the number of iterations is presented figure 19 in appendix D. We can see that the scheme is convergent and that it needs approximatively 5000 iterations for all the residuals to go under 10^{-5}.

The simulation allows us to plot the Mach number distribution inside the nozzle as presented figure 18. We can notice that the shock expected happens in order to provide a subsonic outlet.
The other computed quantities are presented in appendix D. The density, the velocity, the total energy and the pressure distributions are all presented figure 20 as well as the Mach number distribution figure 21. We can notice the effect of the shock with all quantities changing abruptly. We also notice some dispersion effects around the position of the shock.

The same analysis can be done on the results given by the Lax-Wendroff scheme, wich converges after 5000 iterations too. The final Mach distribution is displayed figure 22. The results are given in appendix D. The same conclusions as in the case of the MacCormack scheme can be drawn. However, we can notice figures 24 and 25 that the effects of dispersion (inducing oscillations around the shock) are more important than the results given by the MacCormack scheme.

However, in the case of the Beam-Warming, the results provided are not satisfying. Indeed, we do not obtain the expected behavior with a shock to meet the subsonic outlet condition. The behavior of the fluid is computed as the one of the supersonic outlet case.

Conclusion

This project has allowed us to investigate two different study cases on wich we applied three numerical schemes and various boundary conditions.

For the Sod shock tube, all numerical schemes provide a strong agreement with the analytical solution. Some effects of dispersion can be observerd for the MacCormack and the Lax-Wendroff schemes, and some dissipation for the implicit Beam-Warming scheme.

For the Nozzle, all numerical schemes provide the results expected in the case of a supersonic inlet and a supersonic outlet. However, when we switch to the case with a supersonic inlet and a subsonic outlet, the Beam-Warming scheme does not provide the results expected. The MacCormack and Lax-Wendroff schemes provide good results, showing the shock that is expected.

Therefore, most of the results are really satisfying, showing the effects of various numerical schemes to solve a complex 1D (or quasi-1D) equation : the Euler equation.

References

[1] Cebeci, T., Shao, J., Kafyeke, F., and Laurendeau, E. (2007). *Computational Fluid Dynamics for Engineers: From Panel to Navier-Stokes Methods with Computer Programs*. Springer Berlin Heidelberg.

A Numerical schemes [1]

In the following, $\vec{Q}_i^n$, $\vec{E}_i^n$, and $\vec{S}_i^n$ represent the approximations of the conserved variable vector $\vec{Q}$, the flux vector $\vec{E}$, and the source term vector $\vec{S}$, respectively, at the i-th cell and time level t_n.

Mac-Cormack Scheme

The Mac-Cormack scheme involves two stages: a **predictor step** followed by a **corrector step**. This method is derived from the Taylor expansion of the conserved variable vector $\vec{Q}$:

$$\vec{Q}_i^{n+1} = \vec{Q}_i^n + \Delta t \left(\frac{\partial \vec{Q}}{\partial t}\right)_i^n = \vec{Q}_i^n + \Delta t \left(\vec{S} - \frac{\partial \vec{E}}{\partial x}\right)_i^n = \vec{Q}_i^n + \Delta t \vec{S}_i^n - \Delta t \left(\frac{\partial \vec{E}}{\partial x}\right)_i^n$$

In the predictor step, the solution is advanced using forward differences:

$$\vec{\overline{Q}}_i = \vec{Q}_i^n - \frac{\Delta t}{\Delta x}(\vec{E}_{i+1}^n - \vec{E}_i^n) + \Delta t \vec{S}_i^n \textbf{ (Predictor step)}$$

In the corrector step, backward differences are used to refine the solution:

$$\vec{\vec{\overline{Q}}}_i = \vec{Q}_i^n - \frac{\Delta t}{\Delta x}(\vec{\overline{E}}_i - \vec{\overline{E}}_{i-1}) + \Delta t \vec{\overline{S}}_i \textbf{ (Corrector step)}$$

Here, $\vec{\overline{E}}$ and $\vec{\overline{S}}$ are computed using the predicted variables $\vec{\overline{Q}}$. Finally, the solution at time level $n+1$ is obtained by averaging the results from both steps:

$$\vec{Q}_i^{n+1} = \frac{\vec{\overline{Q}}_i + \vec{\vec{\overline{Q}}}_i}{2}$$

Lax-Wendroff

The Lax-Wendroff scheme is also derived from the Taylor expansion of the conserved variable vector $\vec{Q}$:

$$\vec{Q}_i^{n+1} = \vec{Q}_i^n + \Delta T \left(\frac{\partial \vec{Q}}{\partial t}\right)_i^n + \frac{\Delta T^2}{2}\left(\frac{\partial^2 \vec{Q}}{\partial t^2}\right)_i^n$$

Using the Euler equations [1], we can express the first and second derivatives as:

$$\frac{\partial \vec{Q}}{\partial t} = \vec{S} - \frac{\partial \vec{E}}{\partial x}$$

and

$$\frac{\partial^2 \vec{Q}}{\partial t^2} = \frac{\partial \vec{S}}{\partial t} - \frac{\partial}{\partial x}\left(\frac{\partial \vec{E}}{\partial t}\right) = \frac{\partial \vec{S}}{\partial t} - \frac{\partial}{\partial x}\left(\frac{\partial \vec{E}}{\partial \vec{Q}}\frac{\partial \vec{Q}}{\partial t}\right) = \frac{\partial \vec{S}}{\partial t} - \frac{\partial}{\partial x}\left(\mathbf{A}\left[\vec{S} - \frac{\partial \vec{E}}{\partial x}\right]\right)$$

Substituting these into the Taylor expansion gives:

$$\vec{Q}_i^{n+1} = \vec{Q}_i^n + \Delta T \left(\vec{S} - \frac{\partial \vec{E}}{\partial x}\right)_i^n + \frac{\Delta T^2}{2}\left(\frac{\partial \vec{S}}{\partial t} - \frac{\partial}{\partial x}\left(\mathbf{A}\left[\vec{S} - \frac{\partial \vec{E}}{\partial x}\right]\right)\right)_i^n$$

Expanding this yields:

$$\vec{Q}_i^{n+1} = \vec{Q}_i^n + \Delta T \vec{S}_i^n - \Delta T \left(\frac{\partial \vec{E}}{\partial x}\right)_i^n + \frac{\Delta T^2}{2}\left(\frac{\partial \vec{S}}{\partial t}\right)_i^n - \frac{\Delta T^2}{2}\left(\frac{\partial \mathbf{A}\vec{S}}{\partial x}\right)_i^n + \frac{\Delta T^2}{2}\frac{\partial}{\partial x}\left(\mathbf{A}\frac{\partial \vec{E}}{\partial x}\right)_i^n$$

This equation can be discretized as follows:

$$\vec{Q}_i^{n+1} = \vec{Q}_i^n - \frac{\Delta T}{2\Delta x}\left[\vec{E}_{i+1}^n - \vec{E}_{i-1}^n\right] + \frac{\Delta T^2}{2\Delta x^2}\left[\mathbf{A}_{i+1/2}^n(\vec{E}_{i+1}^n - \vec{E}_i^n) - \mathbf{A}_{i-1/2}^n(\vec{E}_i^n - \vec{E}_{i-1}^n)\right] + \Delta T \vec{S}_i^n + \frac{\Delta T}{2}(\vec{S}_i^n - \vec{S}_i^{n-1}) - \frac{\Delta T^2}{4\Delta x}(\mathbf{A}_{i+1}^n \vec{S}_{i+1}^n - \mathbf{A}_{i-1}^n \vec{S}_{i-1}^n)$$

This formulation constitutes the Lax-Wendroff scheme, where $\mathbf{A} = \frac{\partial \vec{E}}{\partial \vec{Q}}$ denotes the Jacobian matrix.

Implicit Beam-Warming Scheme

The implicit Beam-Warming scheme is derived by discretizing the Euler equations as follows:

$$\frac{\vec{Q}_i^{n+1} - \vec{Q}_i^n}{\Delta T} = -\frac{1}{2\Delta x}\left(\vec{E}_{i+1}^{n+1} - \vec{E}_i^{n+1}\right) + \vec{S}_i^n$$

Using Taylor expansion of the fluxes vector with respect to $\vec{Q}$ yields :

$$\vec{E}_{i+1}^{n+1} = \vec{E}_{i+1}^n + \left(\frac{\partial \vec{E}}{\partial \vec{Q}}\right)_{i+1}^n \left[\vec{Q}_{i+1}^{n+1} - \vec{Q}_{i+1}^n\right] = \vec{E}_{i+1}^n + \mathbf{A}_{i+1}^n \vec{\Delta} Q_{i+1}$$

$$\vec{E}_{i-1}^{n+1} = \vec{E}_{i-1}^n + \left(\frac{\partial \vec{E}}{\partial \vec{Q}}\right)_{i-1}^n \left[\vec{Q}_{i-1}^{n+1} - \vec{Q}_{i-1}^n\right] = \vec{E}_{i-1}^n + \mathbf{A}_{i-1}^n \vec{\Delta} Q_{i-1}$$

Inserting these equations in the discretization leads to :

$$\frac{\vec{\Delta} Q_i}{\Delta T} = -\frac{1}{2\Delta x}\left(\vec{E}_{i+1}^n + \mathbf{A}_{i+1}^n \vec{\Delta} Q_{i+1} - \vec{E}_{i-1}^n - \mathbf{A}_{i-1}^n \vec{\Delta} Q_{i-1}\right) + \vec{S}_i^n$$

Therefore, we have :

$$\vec{\Delta} Q_i + \frac{\Delta T}{2\Delta x}(\mathbf{A}_{i+1}^n \vec{\Delta} Q_{i+1} - \mathbf{A}_{i-1}^n \vec{\Delta} Q_{i-1}) = -\frac{\Delta T}{2\Delta x}\left(\vec{E}_{i+1}^n - \vec{E}_{i-1}^n\right) + \Delta T \vec{S}_i^n$$

This results in a block tridiagonal system to be solved. Typically, fourth-order dissipation is added to the right-hand side of the equation, while second-order dissipation is added to the left-hand side to maintain the block tridiagonal structure. Therefore, the numerical scheme is :

$$\begin{aligned}\vec{\Delta} Q_i + \frac{\Delta T}{2\Delta x}(\mathbf{A}_{i+1}^n \vec{\Delta} Q_{i+1} - \mathbf{A}_{i-1}^n \vec{\Delta} Q_{i-1}) & \\ -\frac{\epsilon_i}{\Delta x^2}\left(\vec{\Delta} Q_{i+1} + \vec{\Delta} Q_{i-1} - 2\vec{\Delta} Q_i\right) &= -\frac{\Delta T}{2\Delta x}\left(\vec{E}_{i+1}^n - \vec{E}_{i-1}^n\right) + \Delta T \vec{S}_i^n \\ &\quad - \frac{\epsilon_e}{\Delta x^4}\left(\vec{Q}_{i-2}^n + \vec{Q}_{i+2}^n + 6\vec{Q}_i^n - 4(\vec{Q}_{i-1}^n + \vec{Q}_{i+1}^n)\right)\end{aligned}$$

The stability of the scheme is assured under the conditions:

$$\epsilon_e \leq \frac{1}{8} \quad \text{and} \quad \epsilon_i \geq 2\epsilon_e.$$

B Results for the shock tube

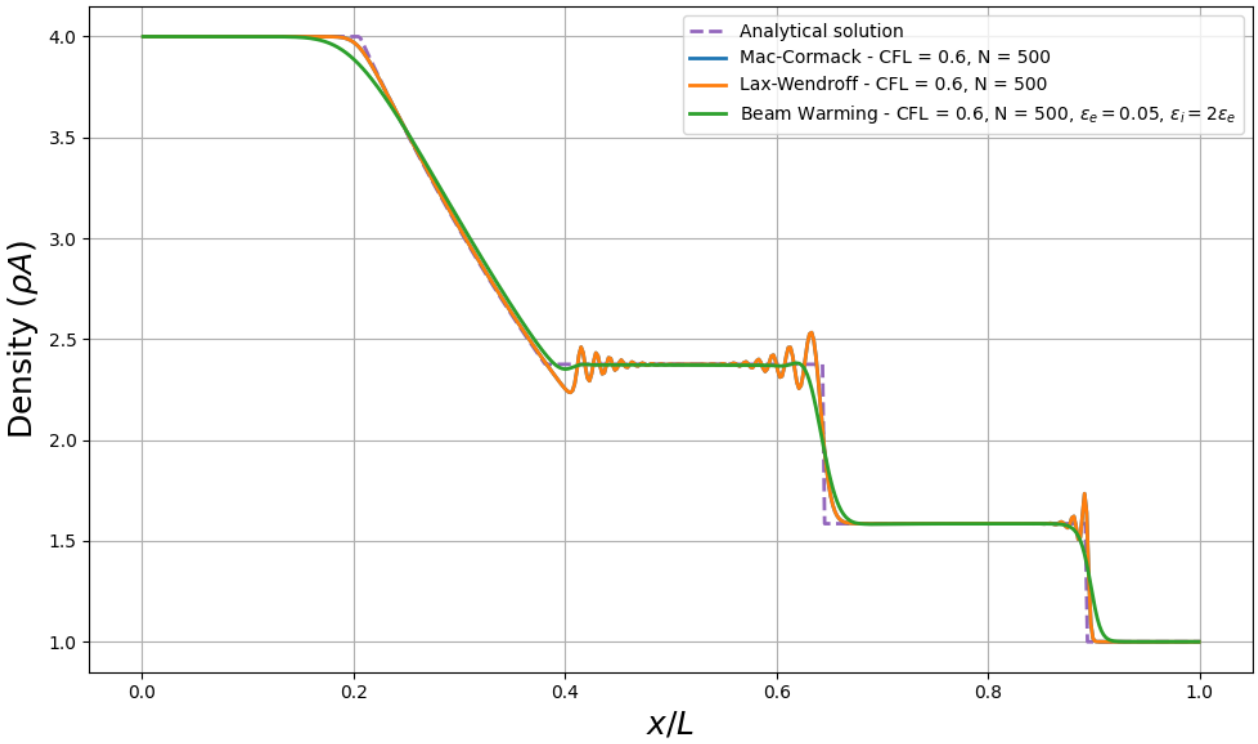

Figure 1: Density profile for the SOD shock tube case at $t = 250$

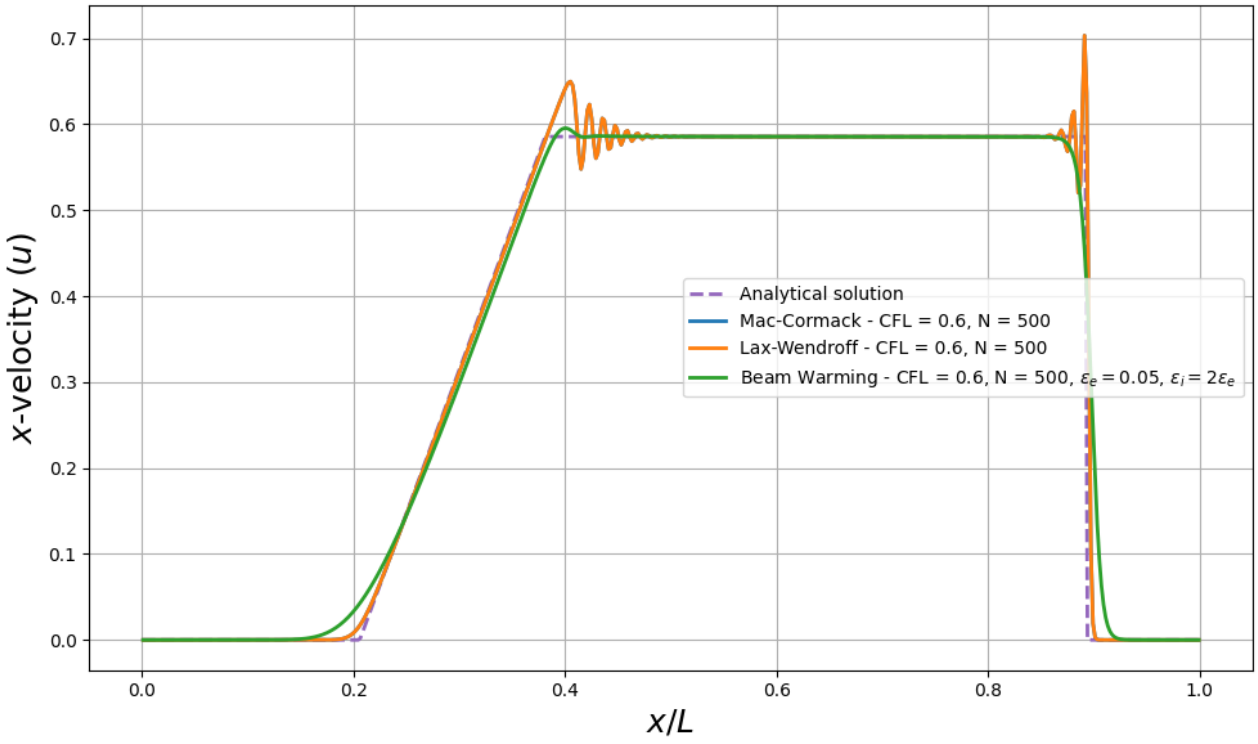

Figure 2: Velocity profile for the SOD shock tube case at $t = 250$

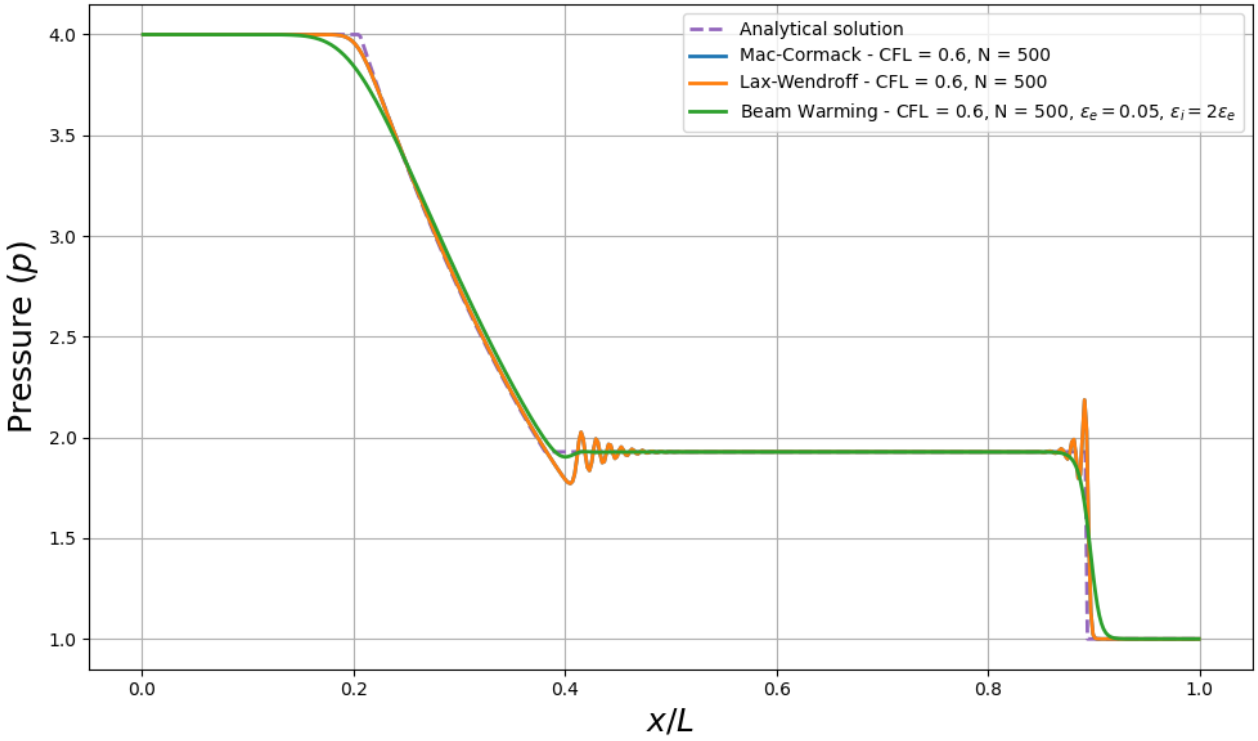

Figure 4: Pressure profile for the SOD shock tube at $t = 250$

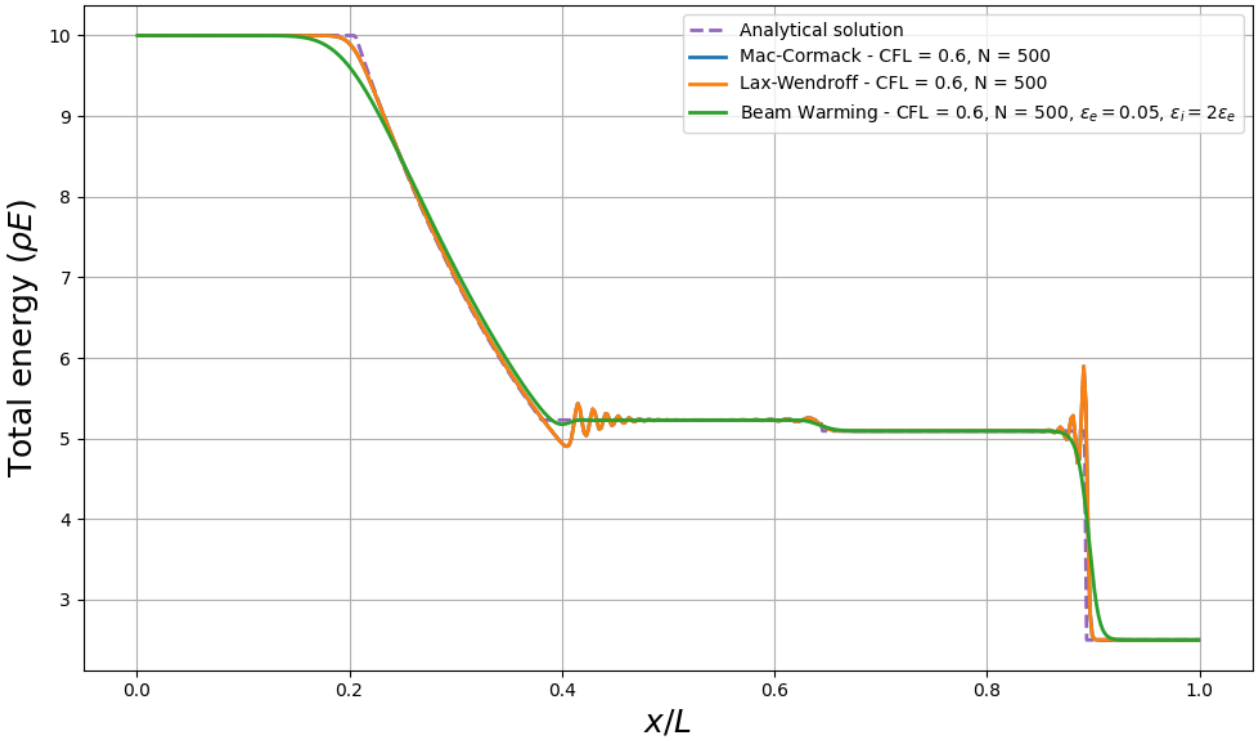

Figure 3: Total energy profile for the SOD shock tube case at $t = 250$

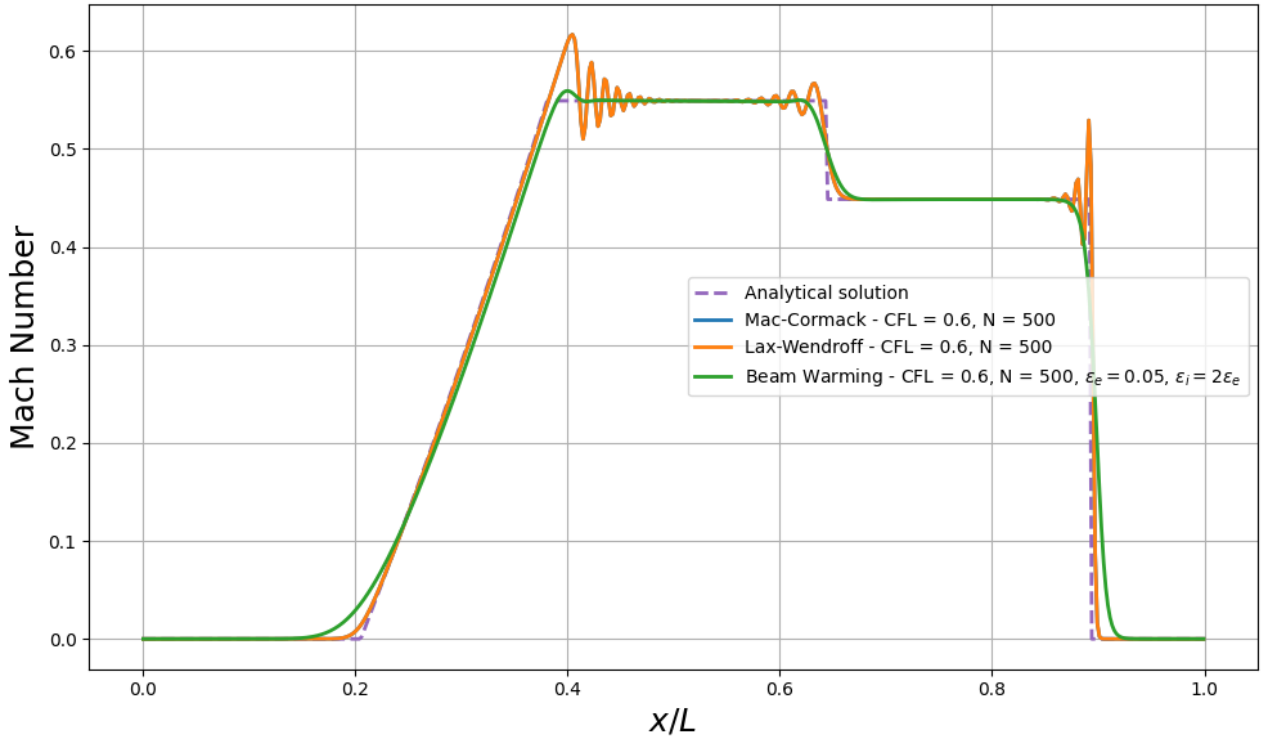

Figure 5: Mach profile for the SOD shock tube at $t = 250$

C Results for the Nozzle : Supersonic inlet - Supersonic outlet

C.1 MacCormack scheme

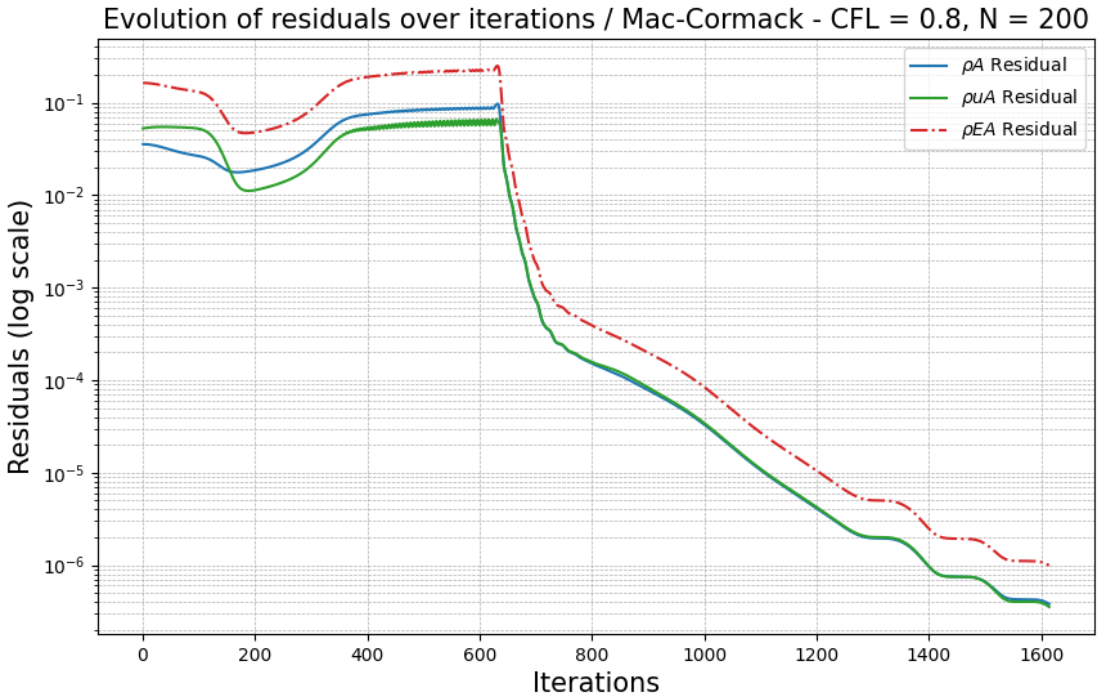

Figure 6: Evolution of residuals over iterations for the Mac-Cormack scheme / Supersonic inlet - Supersonic outlet

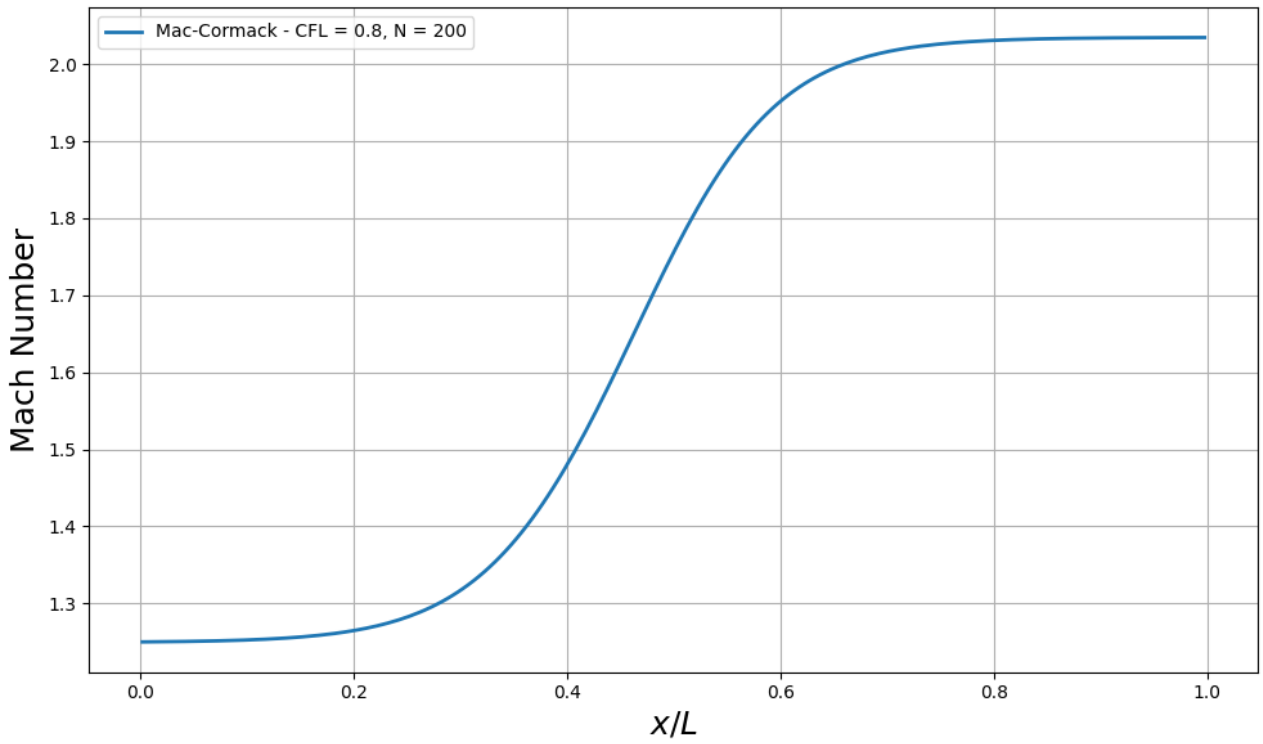

Figure 8: Mach distribution in the nozzle - Mac-Cormack scheme / Supersonic inlet - Supersonic outlet

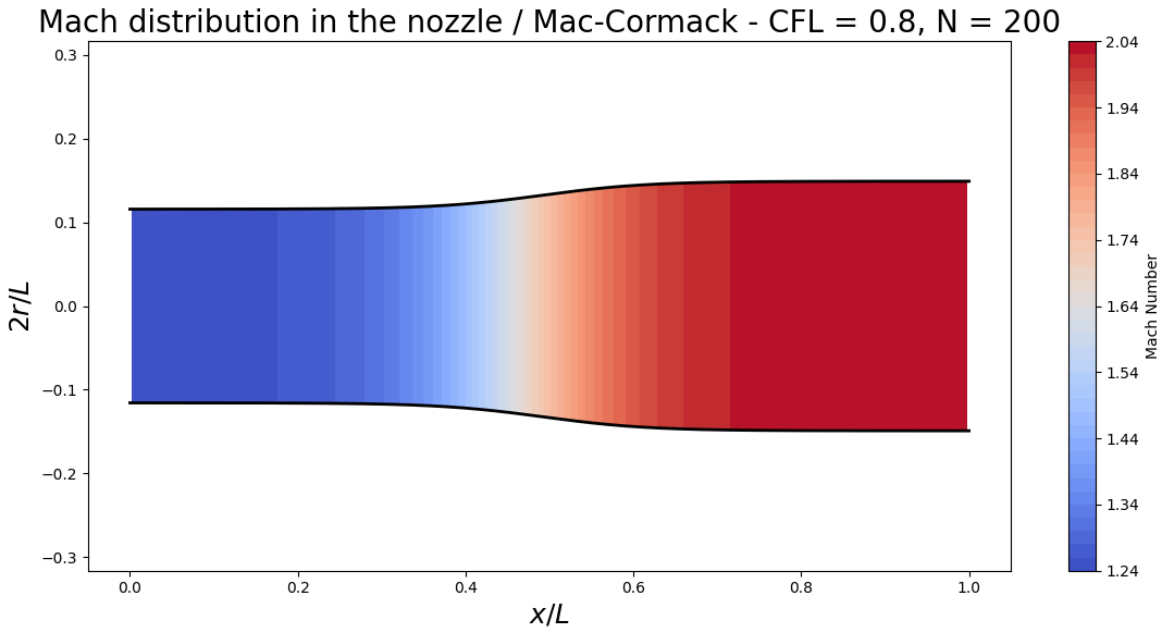

Figure 7: Mach distribution in the nozzle - Mac-Cormack scheme / Supersonic inlet - Supersonic outlet

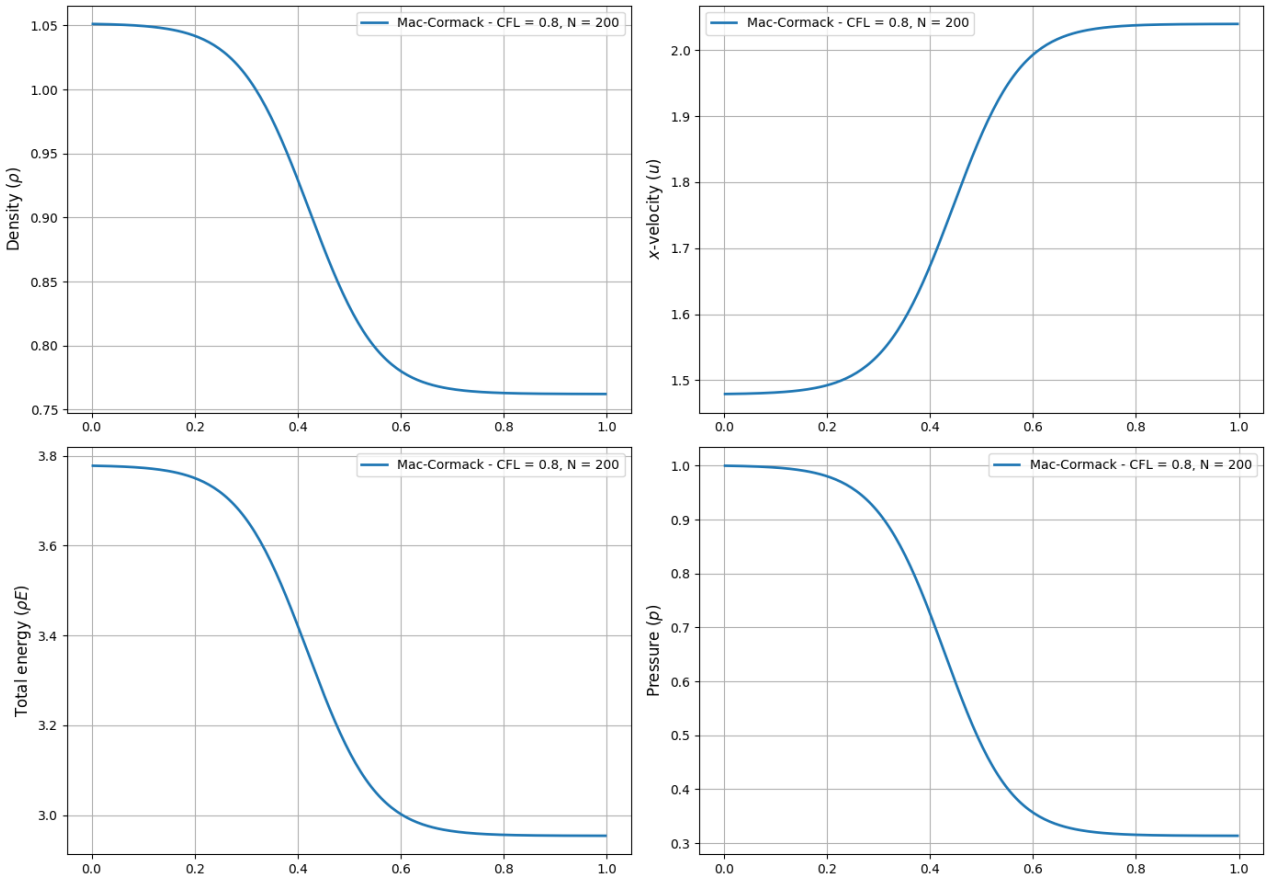

Figure 9: Evolution of density, velocity, pressure and total energy inside the nozzle - Mac Cormack scheme - Supersonic inlet & Supersonic oulet

C.2 Lax-Wendroff scheme

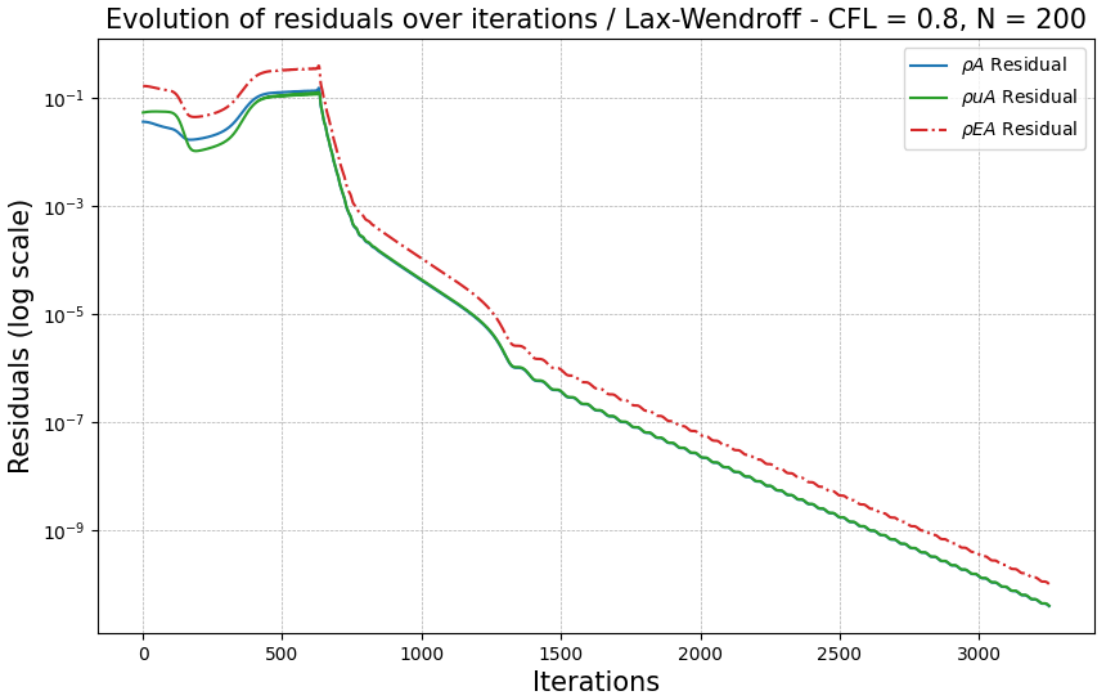

Figure 10: Evolution of residuals over iterations for the Lax-Wendroff scheme / Supersonic inlet - Supersonic outlet

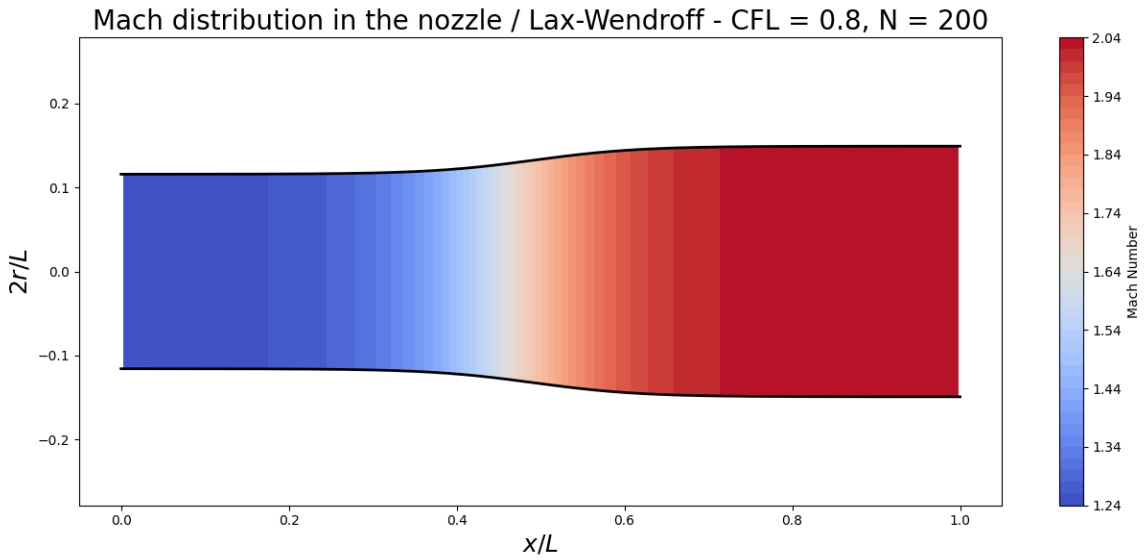

Figure 11: Mach distribution in the nozzle - Lax-Wendroff scheme / Supersonic inlet - Supersonic outlet

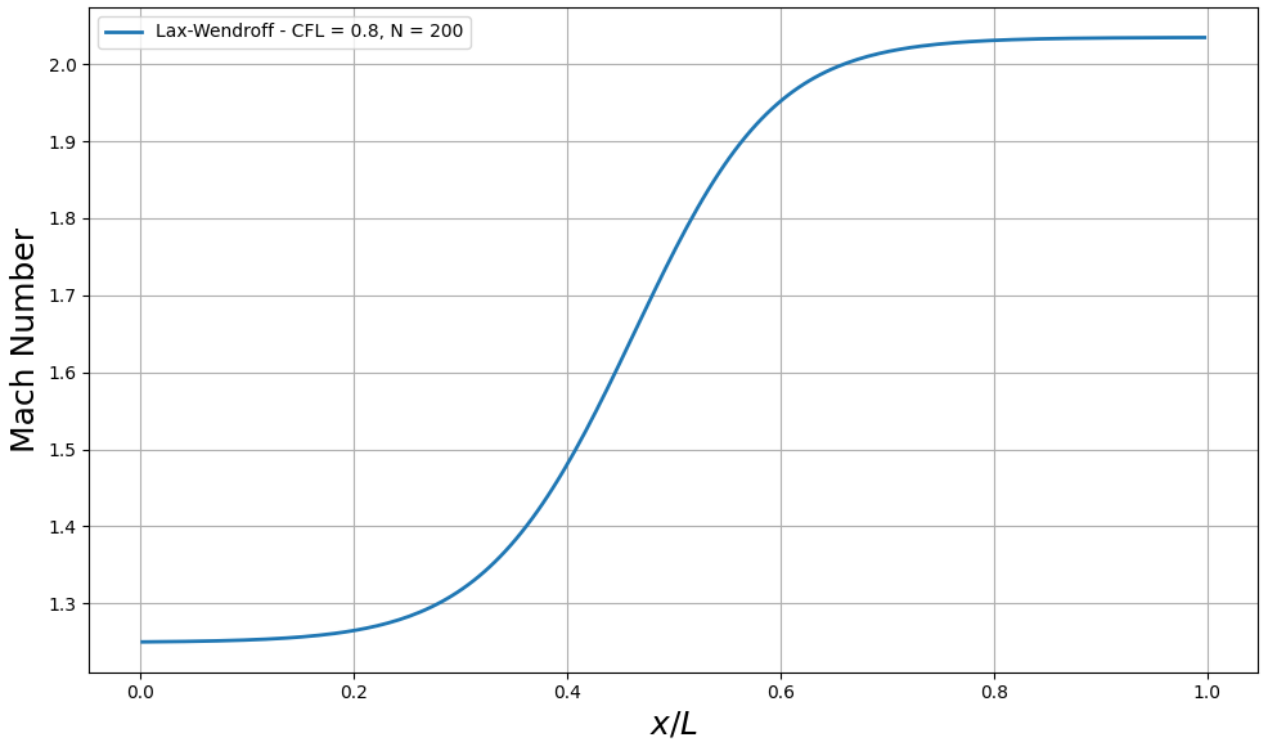

Figure 12: Mach distribution in the nozzle - Lax-Wendroff scheme / Supersonic inlet - Supersonic outlet

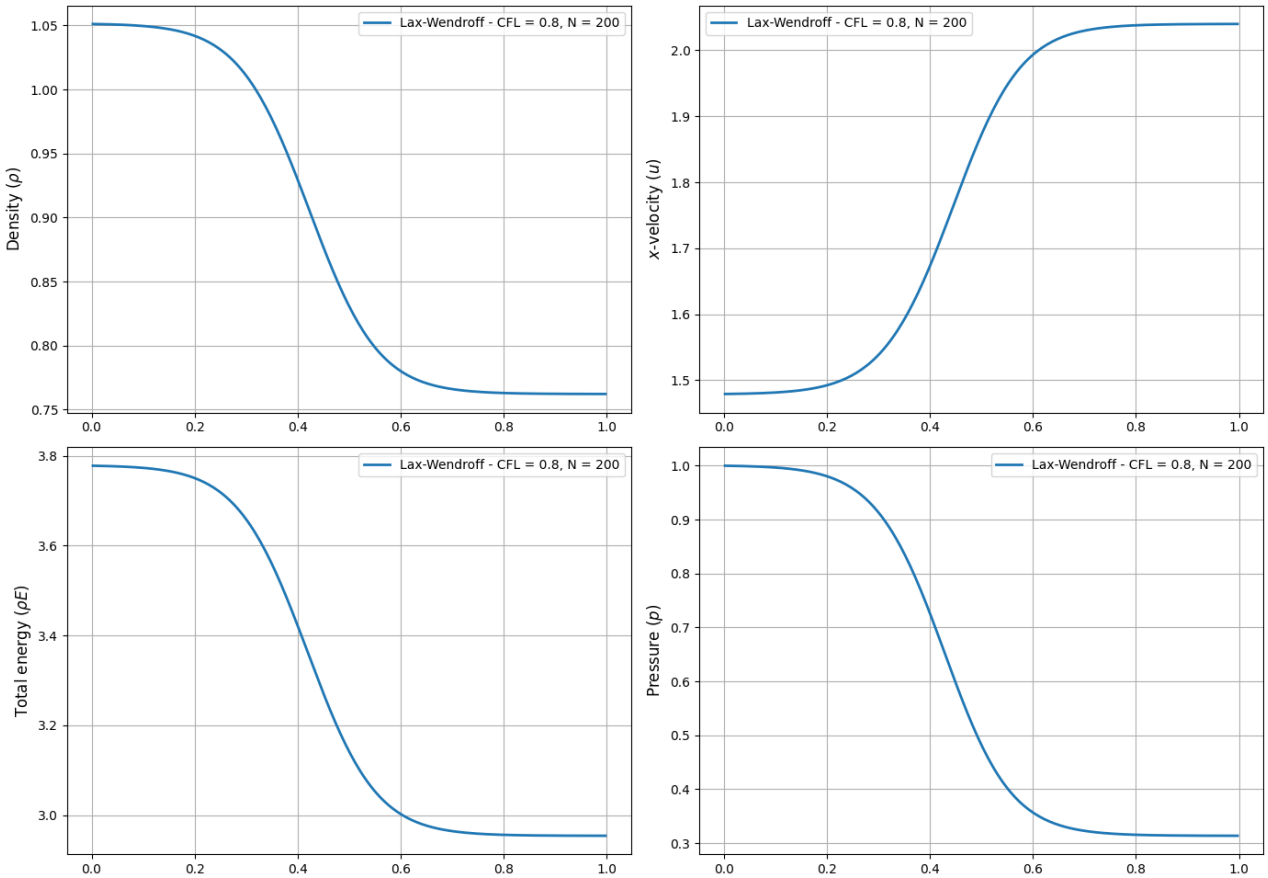

Figure 13: Evolution of density, velocity, pressure and total energy inside the nozzle - Lax-Wendroff scheme - Supersonic inlet & Supersonic oulet

C.3 Implicit Beam-Warming scheme

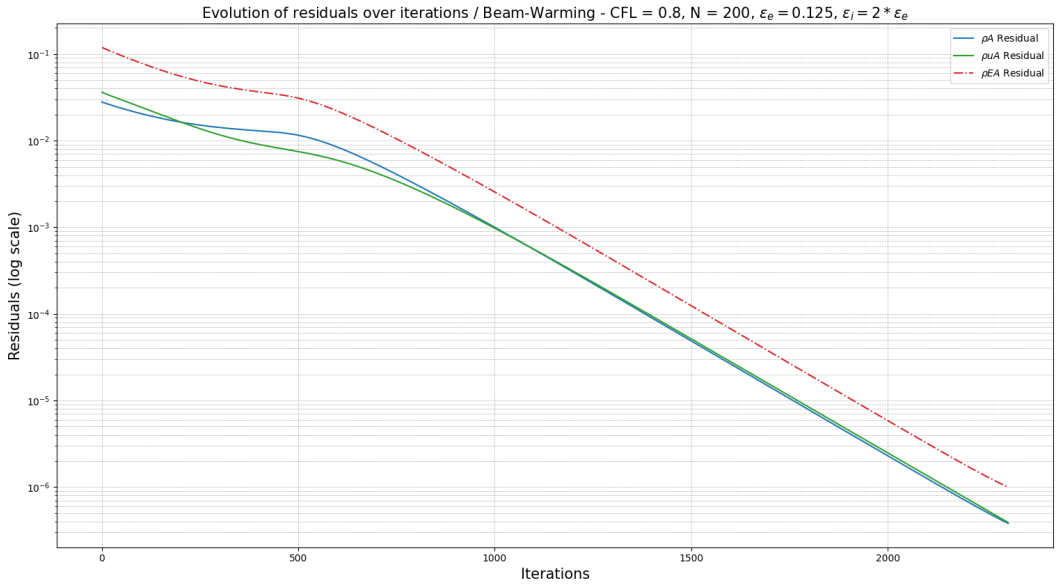

Figure 14: Evolution of residuals over iterations for the Beam-Warming scheme / Supersonic inlet - Supersonic outlet

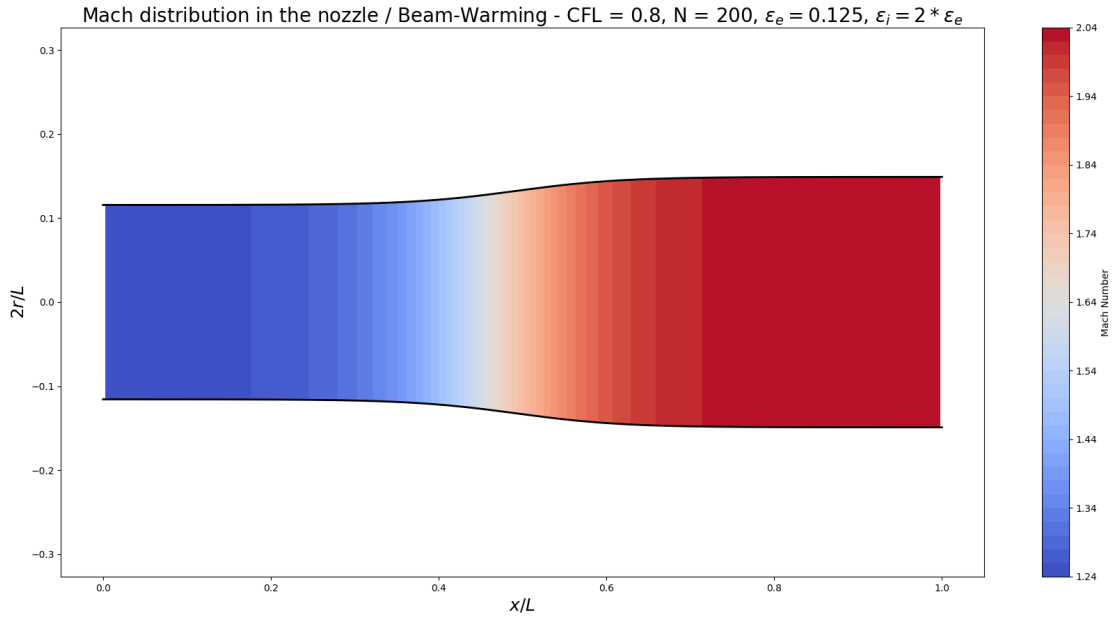

Figure 15: Mach distribution in the nozzle - Beam-Warming scheme / Supersonic inlet - Supersonic outlet

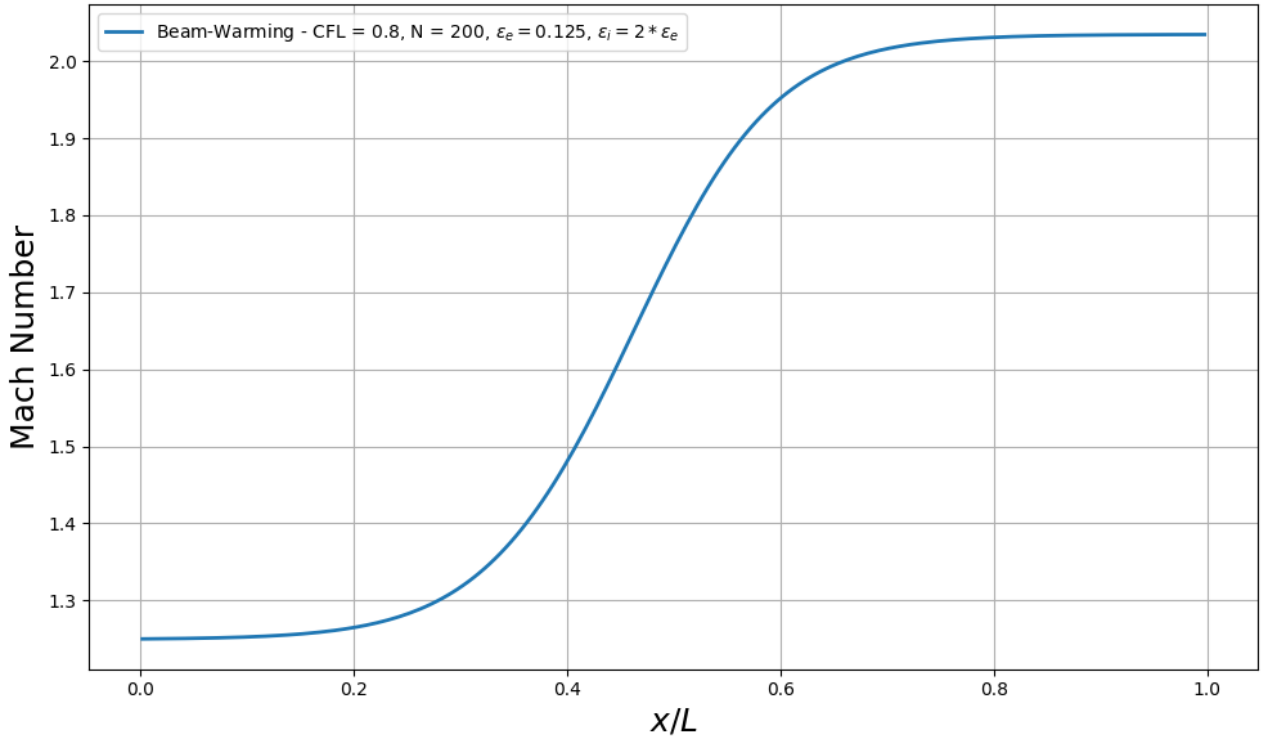

Figure 16: Mach distribution in the nozzle - Beam-Warming scheme / Supersonic inlet - Supersonic outlet

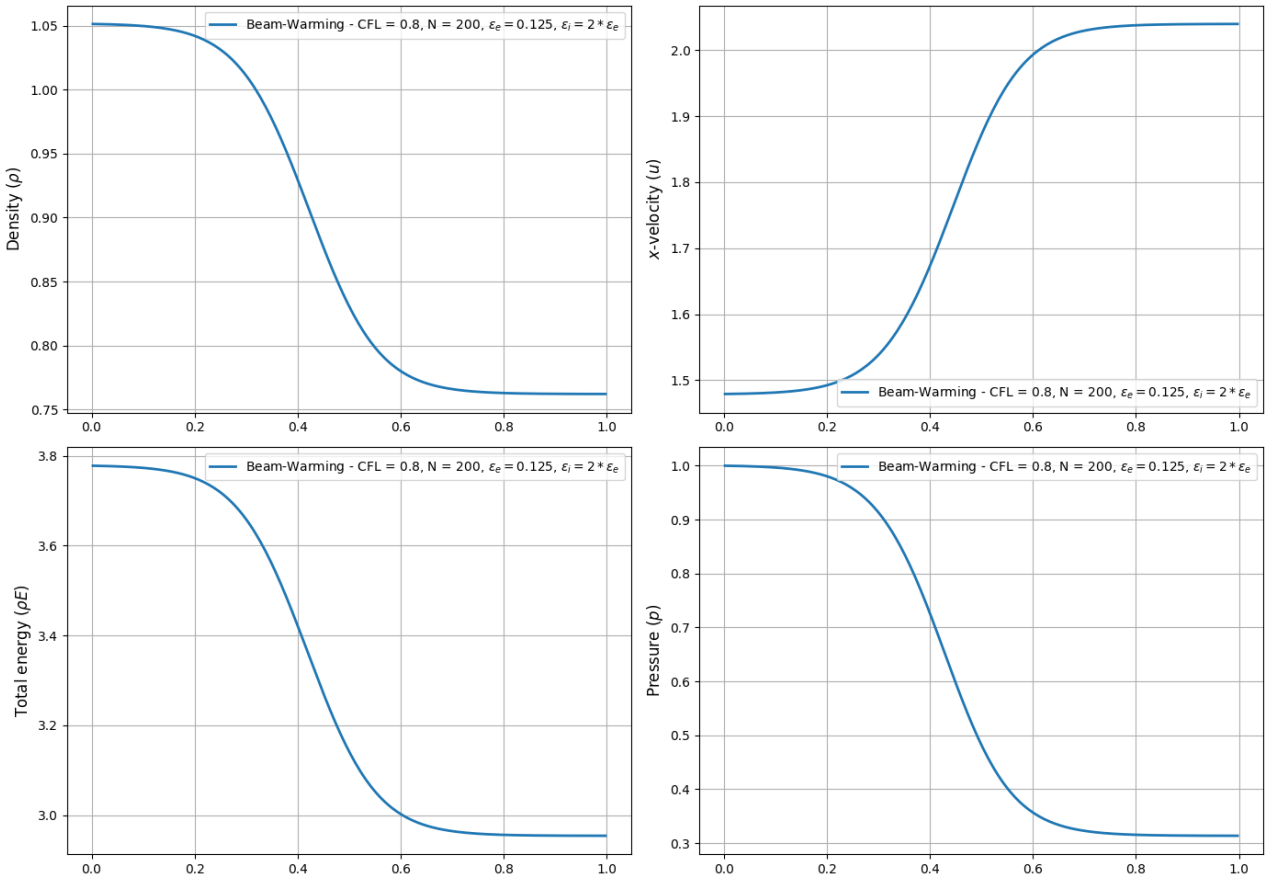

Figure 17: Evolution of density, velocity, pressure and total energy inside the nozzle - Beam-Warming scheme - Supersonic inlet & Supersonic oulet

D Results for the Nozzle : Supersonic inlet - Subsonic outlet

D.1 MacCormack scheme

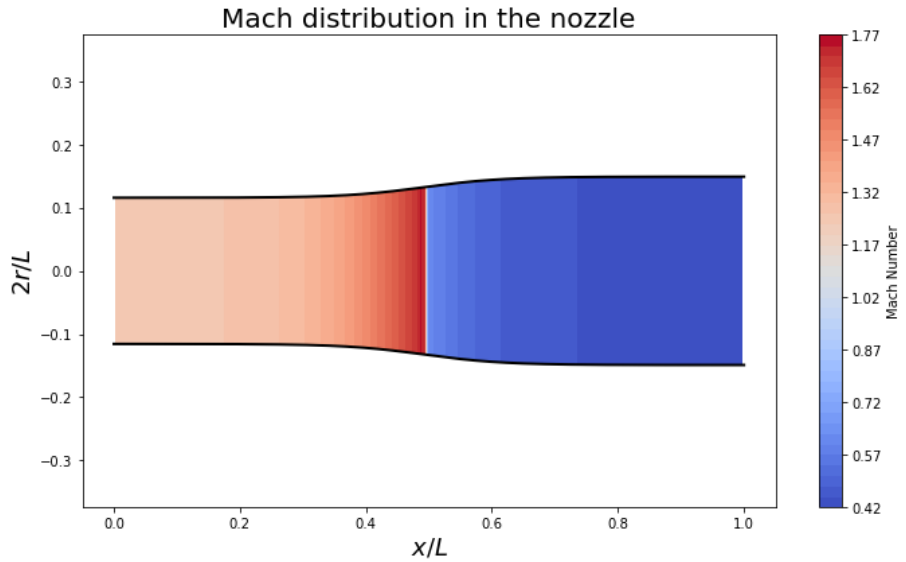

Figure 18: Mach distribution in the nozzle - Mac-Cormack scheme / Supersonic inlet - Subsonic outlet

Figure 19: Evolution of residuals over iterations for the MacCormack scheme / Supersonic inlet - Subsonic outlet

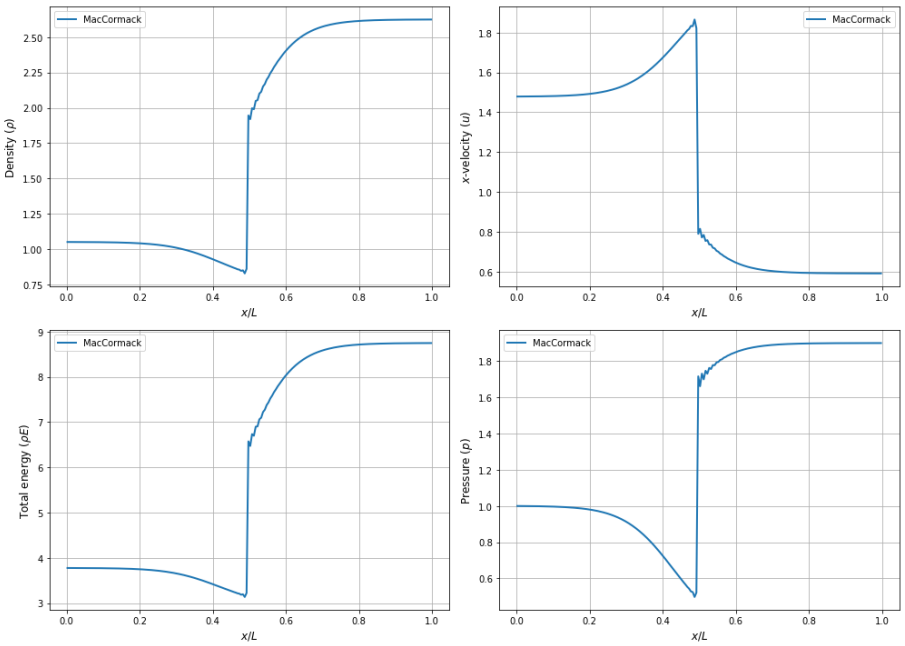

Figure 20: Distributions of density, velocity, energy and pressure for the MacCormack scheme / Supersonic inlet - Subsonic outlet

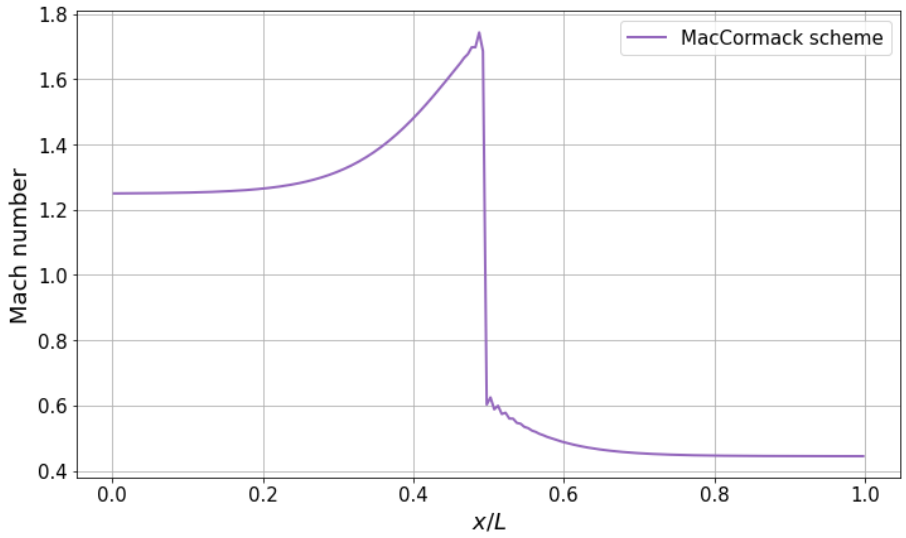

Figure 21: Mach number distribution for the MacCormack scheme / Supersonic inlet - Subsonic outlet

D.2 Lax-Wendroff scheme

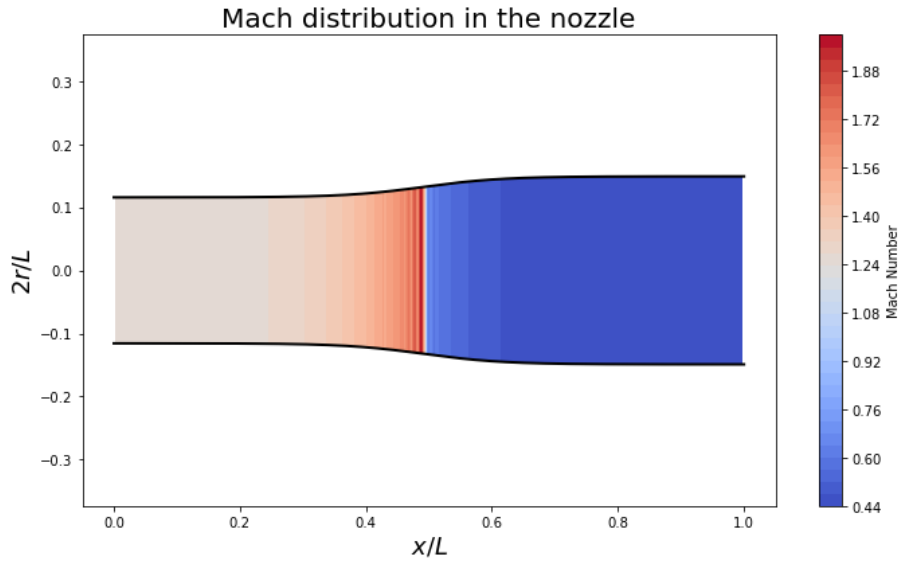

Figure 22: Mach distribution in the nozzle - Lax-Wendroff scheme / Supersonic inlet - Subsonic outlet

Figure 23: Evolution of residuals over iterations for the Lax-Wendroff scheme / Supersonic inlet - Subsonic outlet

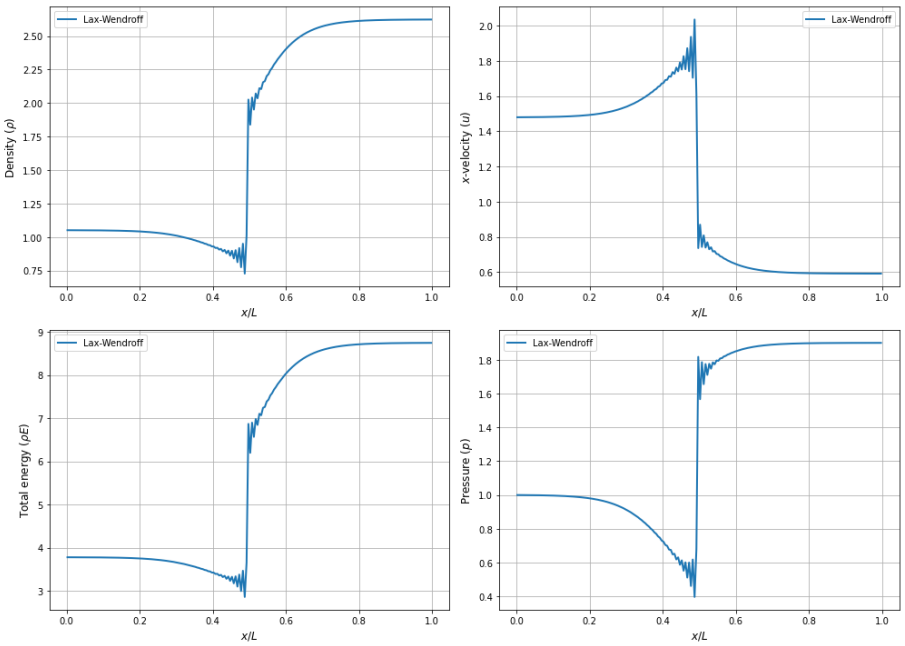

Figure 24: Distributions of density, velocity, energy and pressure for the Lax-Wendroff scheme / Supersonic inlet - Subsonic outlet

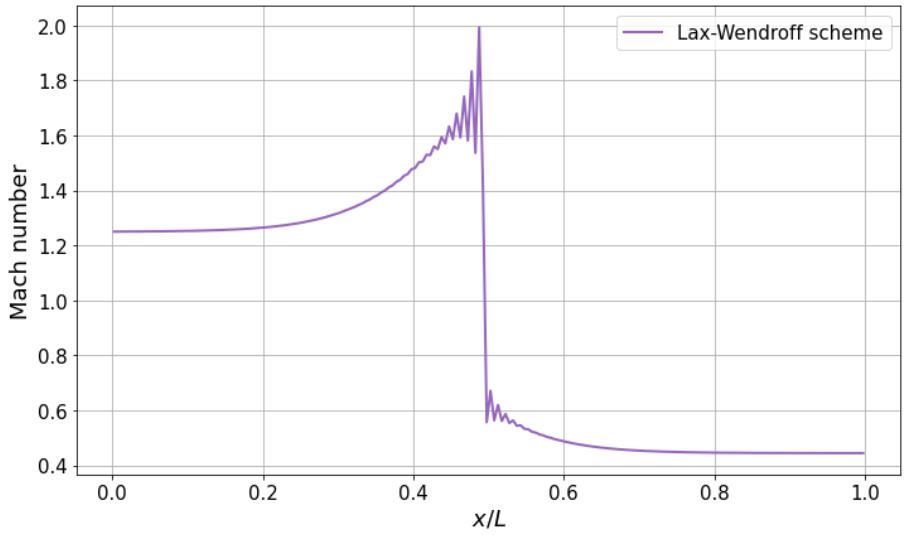

Figure 25: Mach number distribution for the Lax-Wendroff scheme / Supersonic inlet - Subsonic outlet